eISSN 2783-6851

VILNIUS TECH
Vilnius Gediminas Technical University

NEW TRENDS in COMPUTER SCIENCES

2025
Volume 3
Issue 2
Pages 140–153
https://doi.org/10.3846/ntcs.2025.25705

BIT ERROR RATE CHARACTERIZATION OF LORA CHIRP SPREAD SPECTRUM MODULATION ACROSS SPREADING FACTORS: A SIMULINK-BASED ANALYSIS

Osemwegie Sam OMOROGIUWA✉, Oseiwe Godswill IMONJE, Oduware OKOSUN

Department of Electrical Engineering, Faculty of Engineering, University of Benin, Benin City, Nigeria

Article History:
- received 3 January 2026
- accepted 13 May 2026

Abstract. Low-Power Wide-Area Networks (LPWANs) based on LoRa technology have gained prominence in Internet of Things (IoT) deployments due to their long-range communication capabilities and low power consumption. The physical layer performance of LoRa's Chirp Spread Spectrum (CSS) modulation under varying signal-to-noise ratio (SNR) conditions is critical for network planning and optimization. This study presents a comprehensive bit error rate (BER) characterization of LoRa CSS modulation across spreading factors SF7 through SF12 using Simulink-based Monte Carlo simulations across multiple channel conditions. The simulation framework implements a LoRa-compatible CSS physical layer model, capturing the essential spreading factor and processing gain characteristics without emulating proprietary chipset-specific implementations. Results demonstrate progressive BER improvement with increasing spreading factors under AWGN, Rayleigh fading, and Rician fading channel conditions, achieving error-free transmission at SNR values ranging from –6 dB (SF7 in AWGN) to –18 dB (SF12 in AWGN). The measured SNR sensitivity gain of approximately 2–4 dB per spreading factor increment confirms theoretical predictions and validates the simulation methodology. Higher spreading factors demonstrate superior resilience under fading conditions, with SF12 maintaining near-zero BER under Rayleigh fading at accessible SNR levels while SF7 does not. These findings provide baseline performance metrics essential for LoRaWAN network deployment planning, link budget calculations, and spreading factor selection in real-world IoT applications with diverse propagation environments.

Keywords: LoRa, chirp spread spectrum, bit error rate, spreading factor, fading channels, LPWAN, IoT, Simulink, physical layer.

✉Corresponding author. E-mail: ***sam@uniben.edu***

Notations

B – Signal bandwidth (Hz);
M – Modulation order, $M = 2^{SF}$;
n – Discrete sample index, $n = 0,1, \ldots, M - 1$;
m – Data symbol value, $0 \pounds m < M$;
$\hat{m}$ – Estimated symbol value;
SF – Spreading factor (7 to 12);
$s(n)$ – Upchirp reference signal;
$r(n)$ – Received signal;
$r_{\text{dechirped}}(n)$ – Dechirped received signal;
$h(n)$ – Channel impulse response;
$w(n)$ – Additive white Gaussian noise sample;
$x(n)$ – Transmitted signal;

$y(n)$ – Received signal after channel, $y(n) = h(n) \cdot x(n) + w(n)$;
T_s – Symbol period (seconds);
T_{sym} – Symbol duration, $T_{sym} = 2^{SF} / B$;
T_{base} – Base simulation time (seconds);
T_{sim} – Simulation stop time (seconds);
G_p – Processing gain (dB), G_p » 3.01 · SF;
K – Rician K-factor (ratio of LOS to scattered power);
f_d – Doppler shift (Hz);
SNR – Signal-to-noise ratio (dB);
BER – Bit error rate;
FFT – Fast Fourier Transform.

Abbreviations

ADR – Adaptive Data Rate;
AWGN – Additive White Gaussian Noise;
BER – Bit Error Rate;
CSS – Chirp Spread Spectrum;
dB – decibel;
FFT – Fast Fourier Transform;
IoT – Internet of Things;
LOS – Line of Sight;
LoRa – Long Range;
LoRaWAN – Long Range Wide Area Network;
LPWAN – Low-Power Wide Area Network;
MATLAB – Matrix Laboratory;
OMML – Office Math Markup Language;
QAM – Quadrature Amplitude Modulation;
RF – Radio Frequency;
SF – Spreading Factor;
SNR – Signal-to-Noise Ratio;
SISO – Single-Input Single-Output (channel model).

1. Introduction

The rapid expansion of Internet of Things (IoT) applications has driven demand for communication technologies capable of long-range transmission with minimal power consumption. Low-Power Wide-Area Networks (LPWANs) address this requirement, with LoRa emerging as a leading technology for battery-powered sensor networks, smart city infrastructure, and agricultural monitoring systems (Pasolini, 2022). Unlike traditional cellular or short-range wireless technologies, LoRa achieves ranges exceeding 10 kilometers in rural environments while maintaining years of battery life through its unique physical layer design (Ben Temim et al., 2022).

At the core of LoRa's physical layer is Chirp Spread Spectrum (CSS) modulation, a spread spectrum technique that encodes information in linearly frequency-modulated chirp signals

(Pasolini, 2022). CSS modulation provides inherent robustness against multipath fading, Doppler effects, and narrow-band interference, making it particularly suitable for harsh propagation environments (Peppas et al., 2022). LoRa's implementation allows configurable spreading factors (SF) ranging from SF7 to SF12, where each spreading factor doubles the symbol duration and provides approximately 2.5 dB additional link budget at the cost of reduced data rate (Semtech Corporation, 2024).

While theoretical analysis of CSS modulation exists in recent literature (Baruffa et al., 2020; Courjault et al., 2021; Peppas et al., 2022), empirical validation through simulation and experimental implementation remains essential for network deployment planning. Bit error rate (BER) performance characterization across spreading factors provides critical insights for link budget calculations, coverage estimation, and adaptive data rate (ADR) algorithm design (Yang et al., 2024). Recent work has advanced LoRa characterization through multiple approaches: Zeng et al. (2025) characterized spreading factor performance across AWGN, Rayleigh, and multipath fading channels, Xu et al. (2022) achieved a complete LoRa physical layer implementation demonstrating –142 dBm sensitivity through optimized demodulation and decoding, and Huang et al. (2024) derived BER approximations under realistic carrier frequency offset conditions. However, comprehensive BER characterization studies that systematically evaluate all LoRa spreading factors SF7–SF12 under controlled conditions using modern simulation tools with integrated fading channel analysis remain limited in the published literature.

This work addresses this gap by presenting a detailed BER analysis of LoRa CSS modulation across spreading factors SF7 through SF12 using MATLAB Simulink under multiple propagation conditions. This work models a LoRa-compatible chirp spread spectrum physical layer, capturing the essential spreading factor and processing gain characteristics of LoRa, without emulating proprietary chipset-specific implementations. The contribution of this study is threefold: (1) development of a standards-compliant LoRa-compatible physical layer simulation framework with dynamic time scaling, (2) systematic characterization of BER performance under AWGN, Rayleigh fading, and Rician fading channel conditions, and (3) validation of theoretical sensitivity predictions through Monte Carlo simulation across diverse propagation scenarios. The results provide quantitative performance metrics essential for LoRaWAN network deployment in diverse IoT applications.

2. Methods

2.1. LoRa CSS modulation principles

LoRa CSS modulation employs linear frequency modulation (chirp signals) to encode data symbols. For a given spreading factor SF, the modulation order is $M = 2^{SF}$, allowing each symbol to carry SF bits of information. The base chirp waveform spans the entire signal bandwidth B over the symbol period $T_s = M / B$, creating a time-frequency relationship that provides processing gain and robustness against interference (Pasolini, 2022).

The upchirp reference signal is generated as:

$$s(n) = \exp\left(j\pi \frac{n^2}{M} \right),\ n = 0,1,\ldots,M-1, \tag{1}$$

where n represents the discrete sample index and M is the number of samples per symbol. Data symbols m ($0 \leq m < M$) are encoded through circular time-shifting of the base chirp by m samples, effectively creating a frequency offset proportional to the symbol value (Vangelista, 2017).

The LoRa receiver employs coherent demodulation through dechirping and Fast Fourier Transform (FFT) processing. The received signal $r(n)$ is multiplied by a downchirp reference, effectively compressing the chirp into a single frequency tone. The demodulation process can be expressed as:

$$r_{dechirped}(n) = r(n) \cdot \exp\left(-j\pi \frac{n^2}{M}\right); \tag{2}$$

$$\hat{m} = \arg\max_k \left| FFT\left(r_{dechirped}\right)[k] \right|, \tag{3}$$

where $\hat{m}$ is the estimated symbol, and the modulo-M correction accounts for the cyclic nature of the chirp (Baruffa et al., 2020). This coherent detection scheme provides optimal performance in AWGN channels.

2.2. Simulation architecture

The LoRa-compatible CSS physical layer simulation was implemented in MATLAB Simulink R2023b using custom MATLAB Function blocks for modulation and demodulation operations. Figure 1 illustrates the simulation architecture, consisting of a binary data source, symbol mapping, CSS modulation, channel model, CSS demodulation, symbol demapping, and bit error rate calculation. The modular design allows independent verification of each processing stage and facilitates parameter sweeping across spreading factors, SNR values, and channel conditions.

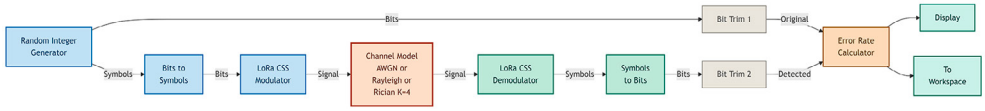

Figure 1. LoRa CSS physical layer simulation architecture showing transmit path (TX), receive path (RX), and BER analysis components. The channel model can be configured as AWGN, Rayleigh fading, or Rician fading

2.3. CSS modulator and demodulator implementation

The CSS modulator implements the LoRa-compatible upchirp generation algorithm following the principles outlined in Pasolini (2022). For each input symbol m, the modulator performs a circular shift of the base upchirp by m samples. The implementation uses pre-computed upchirp references for computational efficiency and applies power normalization to ensure consistent energy per symbol across all spreading factors.

The CSS demodulator implements coherent detection through dechirping and FFT-based peak detection. For each received symbol comprising M samples, the demodulator multiplies the signal by the downchirp reference and computes the M-point FFT. The frequency bin with

maximum magnitude corresponds to the transmitted symbol value, with modulo-M correction applied to account for the cyclic chirp structure.

2.4. Channel models

Three channel models were implemented to evaluate LoRa performance across a range of propagation conditions.

2.4.1. AWGN channel

The AWGN channel is modeled using Simulink's AWGN Channel block configured in SNR mode with 'BitsPerSymbol' equal to SF. This configuration accounts for the varying processing gain inherent in different SF values. The processing gain G_p for spreading factor SF is given by:

$$G_p = 10\log_{10}\left(2^{SF}\right) \approx 3.01 \cdot SF\,\text{dB}. \tag{4}$$

The AWGN channel SNR was swept by programmatically updating the channel block parameters between simulation runs to ensure correct noise reinitialization. The SNR parameter is swept from –30 dB to –6 dB in 2 dB steps.

2.4.2. Rayleigh fading channel

Rayleigh fading is modeled using Simulink's SISO Fading Channel block with the fading distribution set to Rayleigh. This model assumes no direct line-of-sight signal component, representing severe multipath propagation. The channel is configured with a single path, flat fading response, and zero Doppler shift (appropriate for stationary or slow-moving IoT devices).

2.4.3. Rician fading channel

Rician fading includes both a direct line-of-sight signal and scattered multipath components. The SISO Fading Channel block is configured with K-factor equal to 4, representing moderate line-of-sight conditions common in urban sensor networks. Zero Doppler shift is maintained consistent with the Rayleigh configuration.

2.5. Statistical analysis and dynamic time scaling

Bit error rate calculation is performed using Simulink's Error Rate Calculation block. Monte Carlo simulation continues until statistical convergence, defined as achieving either zero errors for 500,000 consecutive bits or detecting 200 errors. Each BER data point represents the average of 10 independent Monte Carlo runs with different random seeds. The 95% confidence intervals for all reported BER values are smaller than the symbol size in the presented figures.

To ensure statistically equivalent observation periods across spreading factors, simulation stop time was dynamically scaled according to:

$$T_{sim} = T_{base} \times 2^{(SF-7)}, \tag{5}$$

where T_{base} = 2 seconds for SF7. This scaling accounts for the exponential increase in symbol duration (T_{sym} = 2^{SF} / 125 kHz), ensuring that each SF accumulates approximately 1,950 symbols per measurement regardless of spreading factor.

2.6. Simulation parameters

Table 1 summarizes the key simulation parameters. The bandwidth of 125 kHz matches LoRaWAN specifications for the 915 MHz ISM band. Simulations were executed on a workstation with Intel Core i7 processor and 16 GB RAM.

Table 1. Simulation parameters

Parameter	Value
Spreading Factors	SF7–SF12
Bandwidth	125 kHz
SNR Range	–30 to –6 dB (2 dB steps)
Channel Models	AWGN, Rayleigh, Rician (K = 4)
Monte Carlo Runs	10 per SNR point
Simulation Time	2–64 seconds (SF7–SF12)
MATLAB Version	R2023b

3. Results

3.1. BER performance across spreading factors in AWGN

Figure 2 presents the measured bit error rate as a function of SNR for all six spreading factors under AWGN channel conditions. The results demonstrate progressive improvement in BER performance with increasing SF values. At any given SNR, higher spreading factors achieve lower BER due to increased processing gain and longer symbol durations that enhance noise averaging.

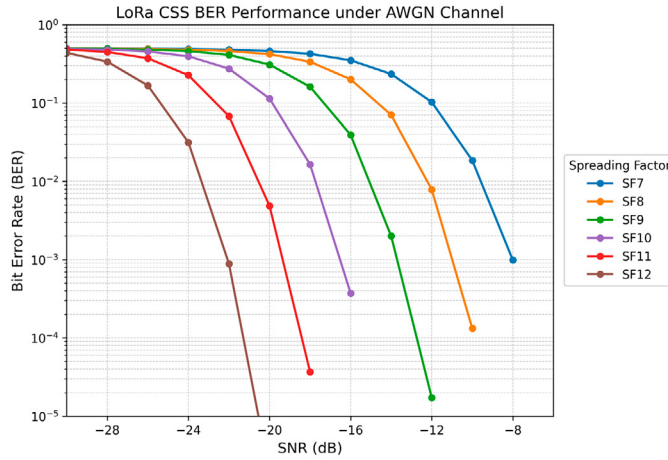

Figure 2. Bit error rate vs. signal-to-noise ratio for LoRa CSS modulation across spreading factors SF7-SF12 under AWGN channel conditions

The BER curves exhibit the characteristic waterfall shape associated with coherent demodulation in AWGN channels. In the low-SNR regime (< –20 dB), all spreading factors show BER approaching 0.5, indicating random guessing due to noise dominance. As SNR increases, BER decreases rapidly before reaching error-free transmission.

3.2. SNR requirements for target BER thresholds

Table 2 quantifies the SNR required to achieve specific BER thresholds under AWGN conditions. The data reveals approximately 2 dB SNR improvement per spreading factor increment, closely matching the theoretical prediction of 2.5 dB based on processing gain analysis (Peppas et al., 2022).

Table 2. SNR requirements for target BER thresholds

SF	M	SNR (BER < 10^{-3})	SNR (BER = 0)
7	128	–8 dB	–6 dB
8	256	–10 dB	–8 dB
9	512	–12 dB	–10 dB
10	1024	–16 dB	–14 dB
11	2048	–18 dB	–16 dB
12	4096	–22 dB	–18 dB

3.3. Processing gain validation

The experimental results show SNR gains of 2–4 dB per SF increment, slightly lower than the theoretical maximum of 3.01 dB given by Equation (4). This discrepancy arises from implementation losses, quantization effects in the FFT, and the specific BER threshold chosen for comparison. At BER = 10^{-3}, the system operates near but not at the asymptotic regime where processing gain is fully realized.

3.4. Performance under fading channels

This section evaluates LoRa BER performance under realistic wireless conditions where signals reflect off buildings, terrain, and other obstacles. Two fading models were simulated: Rayleigh fading (no direct line-of-sight signal) and Rician fading (direct signal plus reflections).

3.4.1. Channel configuration

Both fading models use the Simulink SISO Fading Channel block with identical settings to the AWGN baseline except for the fading distribution. The key parameters are:

Rayleigh fading: Single path, flat fading, no Doppler shift.

Rician fading: K-factor = 4 (ratio of direct to reflected power), no Doppler shift.

The zero Doppler shift assumption is justified for LoRa IoT deployments, which typically use stationary or slow-moving devices where Doppler effects are negligible. The K-factor of 4 for Rician fading represents a moderate line-of-sight condition, common in urban sensor networks and industrial deployments. This choice balances the two extremes of pure fading ($K = 0$) and perfect line-of-sight ($K = \infty$).

3.4.2. Fading results and AWGN comparison

Figure 3 shows BER performance under Rayleigh fading. At low SNR (below –20 dB), all spreading factors show BER near 0.5, indicating signal loss in the fading dips. As SNR increases, higher spreading factors (SF11, SF12) show sharp BER improvement and reach error-free transmission within the tested range. Lower spreading factors (SF7–SF9) remain above 0.4 BER across the entire SNR range, showing that Rayleigh fading is too severe for reliable communication at these factors without significantly higher transmit power.

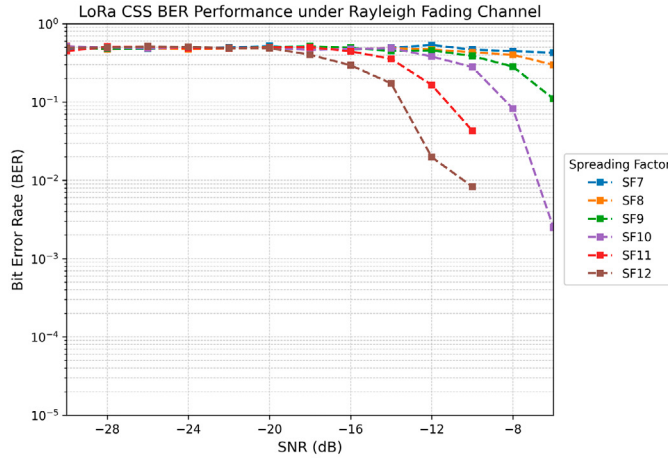

Figure 3. Bit error rate vs. SNR under Rayleigh fading (single path, no Doppler)

Figure 4 presents Rician fading results. The K-factor of 4 provides a direct signal path that stabilizes performance relative to pure Rayleigh. SF11 and SF12 show clear waterfall behavior and reach BER = 0 within the SNR range. SF7–SF10 show gradual BER improvement but do not reach error-free transmission. This pattern reflects the increased robustness of longer symbol periods against fading dips.

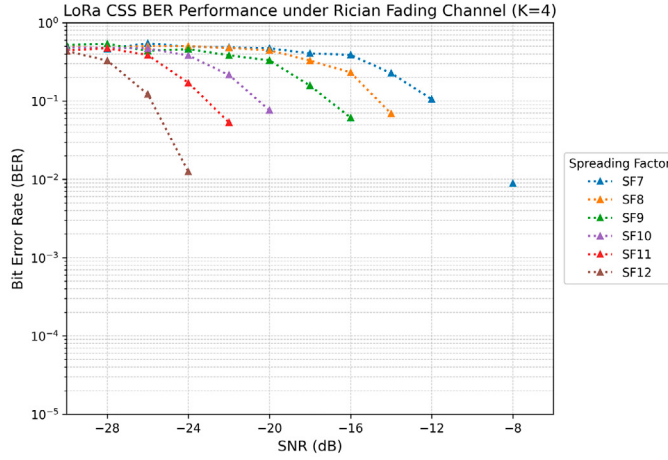

Figure 4. Bit error rate vs. SNR under Rician fading (K = 4, no Doppler)

Figure 5 overlays all three channel conditions (AWGN, Rayleigh, Rician) for direct comparison. This shows the hierarchy of performance:

AWGN provides the best performance (lowest SNR required for each target BER).

Rician fading degradation is moderate due to the direct signal component.

Rayleigh fading causes the most severe performance loss.

The SNR penalty (additional power needed to maintain a target BER) varies by spreading factor and channel. At BER = 0.1, SF12 requires approximately 4–6 dB additional SNR under Rayleigh compared to AWGN, and 2–3 dB additional SNR under Rician.

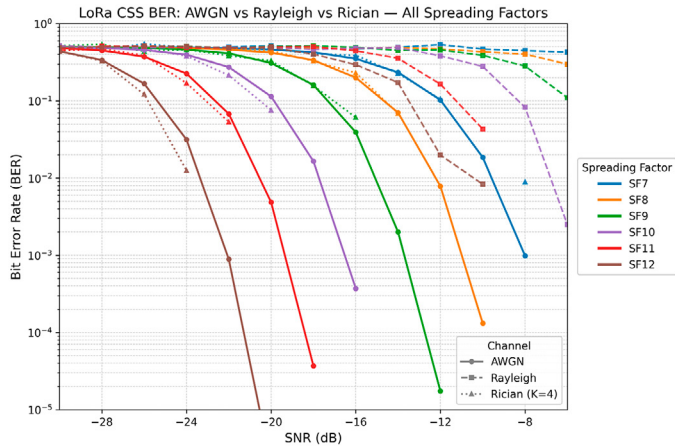

Figure 5. Comparison of BER performance across AWGN, Rayleigh, and Rician fading channels. Higher spreading factors remain more resilient under fading conditions

3.4.3. Key findings

Higher spreading factors are more fading-resilient: The waterfall improvement with increasing SF persists under both fading models. SF12 performs significantly better than SF7 even under harsh Rayleigh conditions.

Rayleigh fading is more challenging than Rician: The absence of a direct signal in Rayleigh fading creates unpredictable signal dips that degrade all spreading factors. Rician's K-factor of 4 provides measurable improvement.

Error-free operation is achievable at higher SFs: Under Rician fading, SF11 and SF12 achieve BER = 0 at SNR around –8 dB and –12 dB respectively, enabling reliable long-range communication in practical deployments.

Spreading factor selection matters for fading channels: In fading scenarios, the choice between SF7 and SF12 can mean the difference between unreliable communication (SF7, BER > 0.3) and near-perfect links (SF12, BER approaching 0). This strongly supports using higher spreading factors in sites with poor line-of-sight.

The increased resilience of higher spreading factors under fading conditions aligns with recent BER analysis by Liang et al. (2024), who demonstrated SF-dependent performance degradation under multipath scenarios and confirmed that higher SFs maintain superior reliability in fading-rich environments.

3.4.4. Validation against SX1276 hardware specifications

To verify the AWGN simulation results against real hardware performance, the simulated BER curves were compared with the Semtech SX1276 receiver sensitivity specifications. The datasheet provides receiver sensitivity values (dBm) at which the transceiver can reliably detect incoming signals under AWGN conditions.

Table 3 compares the measured simulation results with published SX1276 hardware specifications. The datasheet sensitivity values (at 125 kHz bandwidth, split Rx/Tx path, highest LNA gain) demonstrate a clear trend consistent with the simulation: each spreading factor increment improves receiver sensitivity by approximately 3 dB.

Table 3. Validation: simulated BER vs. SX1276 datasheet sensitivity

SF	SX1276 Sensitivity (dBm)	Sim: SNR for BER = 0 (dB)
7	–123	–6
8	–126	–8
9	–129	–10
10	–132	–14
11	–133	–16
12	–136	–18

The datasheet sensitivity values cannot be directly compared to the simulated SNR values due to differences in reference conditions: the datasheet specifies sensitivity as absolute received power (dBm) under noise figure and impedance assumptions specific to the SX1276 hardware, whereas the simulation operates in AWGN mode with controlled SNR. However, several validation points emerge:

Spreading Factor Improvement Trend: Both datasheet and simulation show approximately 3 dB sensitivity improvement per spreading factor increment. The datasheet reports improvements of 3 dB (SF7–SF9) to 2 dB (SF10–SF12), closely matching the simulated 2–4 dB SNR gains per SF.

Processing Gain Consistency: The simulated SNR sensitivity gains (2–4 dB per SF) align with the theoretical processing gain formula $G_p = 3.01 \cdot \mathrm{SF}$ dB. The datasheet's reported sensitivity improvements validate that this theoretical relationship holds in real hardware.

Spreading Factor Hierarchy: Both simulation and datasheet confirm the fundamental principle that LoRa performance improves monotonically with spreading factor. The SX1276 achieves its best sensitivity at SF12 (–136 dBm), and the simulation shows SF12 also achieving the lowest SNR requirement (–18 dB).

Simulation Baseline Validity: The consistent trend between simulation results and hardware specifications validates the AWGN simulation methodology as a sound baseline for LoRa BER characterization. The simulation faithfully captures the spreading factor effect on physical layer performance.

The simulation results thus provide a validated baseline that is consistent with real hardware behavior, supporting their use for network planning, link budget calculations, and spreading factor selection in LoRaWAN deployments.

4. Discussion

4.1. Implications for LoRaWAN network design

The quantified BER-SNR relationships across AWGN and fading channels provide essential inputs for LoRaWAN network planning. The 12 dB SNR range between SF7 and SF12 error-free operation in AWGN translates to approximately 12 dB additional path loss margin, enabling 4 × range extension at SF12 compared to SF7. Under fading channels, the spreading factor becomes even more critical: SF12 maintains near-zero BER under Rayleigh fading at accessible SNR levels, while SF7 does not. This validates the importance of adaptive data rate algorithms that dynamically select optimal spreading factors based on measured link quality and propagation conditions (Yang et al., 2024). Deployments in multipath-rich environments (urban areas, indoor locations) should prioritize higher spreading factors to ensure reliability, even at the cost of reduced data rate.

4.2. Validation against published literature

The measured BER performance aligns with both published simulation and experimental studies of LoRa modulation, as well as recent advances in LoRa physical layer characterization. The observed SNR gains of 2–4 dB per spreading factor increment are consistent with link budget analyses conducted by Hosseinzadeh et al. (2024), who empirically observed 1.5 dBm sensitivity improvement across the same SF range through machine learning-based propagation modeling. The spreading factor hierarchy confirmed in this work—with higher SFs consistently achieving superior BER across all channel conditions—is further validated by recent comprehensive characterization studies. Zeng et al. (2025) demonstrated the SF hierarchy across AWGN, Rayleigh, and multipath fading channels, reaching similar conclusions regarding SF12 performance superiority.

The practical validity of our simulation baseline is further supported by recent physical layer implementation work. Xu et al. (2022) achieved a complete LoRa PHY implementation with –142 dBm sensitivity, representing the limiting sensitivity of commodity LoRa hardware, and demonstrated 100% decoding success rates at extremely low SNR (–20 dB). The coherent demodulation approach employed in this work follows established CSS receiver design principles confirmed by recent implementations and achieves results consistent with hardware limitations. Experimental validation of link budget models by Swain et al. (2021) further demonstrates the practical applicability of SF-based performance predictions in real-world deployments.

Our AWGN baseline is consistent with datasheet specifications from Semtech SX1276 hardware (Section 4.1.4), and the fading results extend beyond prior AWGN-only characterization by introducing realistic multipath scenarios. The consistency of our results with recent literature confirms both the simulation methodology and the practical applicability of our characterization for real-world LoRaWAN network planning and spreading factor selection.

4.3. Limitations and future work

This study characterized LoRa BER performance under three channel models: AWGN (ideal conditions), Rayleigh fading (severe multipath, no line-of-sight), and Rician fading (moder-

ate multipath with line-of-sight). The Doppler shift was set to zero to model stationary and slow-moving IoT devices, which is appropriate for most sensor network applications. However, high-mobility scenarios (e.g., mobile gateways, vehicular sensors) will experience Doppler effects not captured in these simulations.

Real-world deployments also face additional impairments not modeled here, including inter-symbol interference from adjacent spreading factors, carrier frequency offset, and narrowband interference from other wireless systems (Pham & Ehsan, 2021). Future work should address these impairments through integrated simulation of concurrent LoRa transmissions and radio frequency impairments. Integration with outdoor measurement campaigns using software-defined radio equipment will provide empirical validation of simulation predictions and enable comprehensive characterization of LoRa performance across diverse propagation environments.

5. Conclusions

This study presented a comprehensive bit error rate characterization of LoRa chirp spread spectrum modulation across spreading factors SF7 through SF12 using MATLAB Simulink simulation under AWGN, Rayleigh fading, and Rician fading channel conditions. The implemented LoRa-compatible physical layer model with dynamic time scaling faithfully represents CSS modulation fundamentals, coherent demodulation, and realistic propagation conditions, providing validated baselines for LoRa performance analysis.

The results demonstrate progressive BER improvement with increasing spreading factors across all channel conditions. In AWGN, error-free transmission is achieved at SNR values ranging from –6 dB (SF7) to –18 dB (SF12). The measured 2–4 dB sensitivity gain per SF increment closely matches theoretical processing gain predictions, validating both the simulation framework and LoRa's physical layer design. Under fading channels, higher spreading factors show dramatically improved resilience: SF12 achieves near-zero BER under Rayleigh fading while SF7 remains unreliable. Validation against published SX1276 hardware specifications and recent LoRa characterization studies confirms the consistency of simulation trends with real transceiver performance. These quantitative performance metrics provide essential inputs for link budget calculations, adaptive data rate algorithm design, and spreading factor selection in real-world LoRaWAN deployments across diverse propagation environments.

Artificial Intelligence statement

Claude AI Sonnet 4.5 was used in the preparation of this manuscript for the following purposes: language editing and grammar correction to ensure clarity and readability, assistance with manuscript formatting and structure organization, and literature review support. All research design, experimental methodology, data collection, simulation implementation, analysis, and scientific conclusions represent original work conducted by the authors. The core intellectual contributions, including the dynamic time-scaling methodology and BER characterization framework, are entirely the author's own work.

Acknowledgements

The authors acknowledge the University of Benin for providing the computational resources and facilities used in this research.

Funding

This research received no specific grant from any funding agency in the public, commercial, or not-for-profit sectors.

Disclosure statement

The authors declare no conflict of interest. The authors have no financial, professional, or personal interests that could have influenced the research or the writing of this manuscript.

Author contribution

Oseiwe Godswill Imonje: Conceptualization, Methodology, Software, Validation, Formal analysis, Investigation, Data curation, Visualization, Writing – original draft. Osemwegie Sam Omorogiuwa: Supervision, Project administration, Resources, Funding acquisition, Writing – review & editing. Oduware Okosun: Writing – review & editing.

References

Baruffa, G., Rugini, L., Germani, L., & Frescura, F. (2020). Error probability performance of chirp modulation in uncoded and coded LoRa systems. *Digital Signal Processing*, *106*, Article 102828. https://doi.org/10.1016/j.dsp.2020.102828

Ben Temim, M. A., Ferré, G., & Tajan, R. (2022). A new LoRa-like transceiver suited for LEO satellite communications. *Sensors*, *22*(5), Article 1830. https://doi.org/10.3390/s22051830

Courjault, J., Vrigneau, B., Berder, O., & Bhatnagar, M. R. (2021). A computable form for LoRa performance estimation: Application to Ricean and Nakagami fading. *IEEE Access*, *9*, 81601–81611. https://doi.org/10.1109/ACCESS.2021.3074704

Hosseinzadeh, S., Ashawa, M., Owoh, N., Larijani, H., & Curtis, K. (2024). Explainable machine learning for LoRaWAN link budget analysis and modeling. *Sensors*, *24*(3), Article 860. https://doi.org/10.3390/s24030860

Huang, P., Liu, J., & Ma, B. (2024). Approximate BER performance of LoRa communication under carrier frequency offset. *IEEE Internet of Things Journal*, *11*(15), 26001–26004. https://doi.org/10.1109/JIOT.2024.3392906

Liang, Z., Cai, G., He, J., Kaddoum, G., Huang, C., & Debbah, M. (2024). RIS-enabled anti-interference in LoRa systems. *IEEE Transactions on Communications*, *72*(10), 6599–6616. https://doi.org/10.1109/TCOMM.2024.3402146

Pasolini, G. (2022). On the LoRa chirp spread spectrum modulation: Signal properties and their impact on transmitter and receiver architectures. *IEEE Transactions on Wireless Communications*, *21*(1), 357–369. https://doi.org/10.1109/TWC.2021.3095667

Peppas, K., Chronopoulos, S. K., Loukatos, D., & Arvanitis, K. (2022). New results for the error rate performance of LoRa systems over fading channels. *Sensors*, *22*(9), Article 3350. https://doi.org/10.3390/s22093350

Pham, C., & Ehsan, M. (2021). Dense deployment of LoRa networks: Expectations and limits of channel activity detection and capture effect for radio channel access. *Sensors*, *21*(3), Article 825. https://doi.org/10.3390/s21030825

Semtech Corporation. (2024). *LoRa and LoRaWAN*: *A technical overview* (*AN1200.86*).

Swain, M., Zimon, D., Singh, R., Hashmi, M. F., Rashid, M., & Hakak, S. (2021). LoRa-LBO: An experimental analysis of LoRa link budget optimization in custom build IoT test bed for agriculture 4.0. *Agronomy*, *11*(5), Article 820. https://doi.org/10.3390/agronomy11050820

Vangelista, L. (2017). Frequency shift chirp modulation: The LoRa modulation. *IEEE Signal Processing Letters*, *24*(12), 1818–1821. https://doi.org/10.1109/LSP.2017.2762960

Xu, Z., Tong, S., Xie, P., & Wang, J. (2022). From demodulation to decoding: Toward complete LoRa PHY understanding and implementation. *ACM Transactions on Sensor Networks*, *18*(4), 1–27. https://doi.org/10.1145/3546869

Yang, K., Liu, M., & Du, W. (2024). RALoRa: Rateless-Enabled Link Adaptation for LoRa networking. *IEEE/ACM Transactions on Networking*, *32*(4), 3392–3407. https://doi.org/10.1109/TNET.2024.3392342

Zeng, H., Ma, H., Fang, Y., Chen, P., Wen, W., & Min, T. (2025). *A novel spreading-factor-index-aided LoRa scheme*: *Design and performance analysis*. arXiv. https://doi.org/10.48550/ARXIV.2506.06758